Improving image contrast in fluorescence microscopy with nanostructured substrates

Maia Brunstein,[1] Andrea Cattoni,[1] Laura Estrada,[2] and Alejandro M. Yacomotti[1,*]

[1]*Laboratoire de Photonique et de Nanostructures, CNRS, Université Paris-Saclay, route de Nozay, F-91460 Marcoussis, France*

[2]*Quantum Electronics Lab, Dpto. de Física. FCEN, Universidad de Buenos Aires, and IFIBA, Conicet, Pabellón 1, Ciudad Universitaria, 1428 Buenos Aires, Argentina*

[*]*alejandro.giacomotti@lpn.cnrs.fr*

Abstract: Metallic and dielectric nanostructures can show sharp contrasted resonances, sensitive to the environment, and high field enhancement in sub-wavelength volumes. For this reason, these structures are commonly used as molecular sensors. Only few works have focused on their application in optical microscopy, in particular in superresolution. In this work we have designed, fabricated and optically tested a nanostructured TiO_2 substrate, fabricated by direct embossing of TiO_2 derived film, as a substrate for fluorescence microscopy. Moreover, using numerical simulations, we have compared the signal to background noise with respect to other metallo-dielectric structures. We show that the TiO_2 structure is a good candidate for reducing the thickness of the fluorescence excitation down to ~100 nm. Therefore, this substrate can be used to obtain Total Internal Reflection (TIRF) axial resolution without a TIRF-Microscopy system.

OCIS codes: (180.2520) Fluorescence microscopy; (110.2945) Illumination design; (230.5750) Resonators.

References and links

1. M. J. Levene, J. Korlach, S. W. Turner, M. Foquet, H. G. Craighead, and W. W. Webb, "Zero-mode waveguides for single-molecule analysis at high concentrations," Science **299**(5607), 682–686 (2003).
2. A. Cattoni, P. Ghenuche, A. M. Haghiri-Gosnet, D. Decanini, J. Chen, J. L. Pelouard, and S. Collin, "λ^3/1000 plasmonic nanocavities for biosensing fabricated by soft UV nanoimprint lithography," Nano Lett. **11**(9), 3557–3563 (2011).
3. D. Punj, M. Mivelle, S. B. Moparthi, T. S. van Zanten, H. Rigneault, N. F. van Hulst, M. F. García-Parajó, and J. Wenger, "A plasmonic 'antenna-in-box' platform for enhanced single-molecule analysis at micromolar concentrations," Nat. Nanotechnol. **8**(7), 512–516 (2013).
4. I. D. Block, P. C. Mathias, N. Ganesh, S. I. Jones, B. R. Dorvel, V. Chaudhery, L. O. Vodkin, R. Bashir, and B. T. Cunningham, "A detection instrument for enhanced-fluorescence and label-free imaging on photonic crystal surfaces," Opt. Express **17**(15), 13222–13235 (2009).
5. N. Ganesh, W. Zhang, P. C. Mathias, E. Chow, J. A. N. T. Soares, V. Malyarchuk, A. D. Smith, and B. T. Cunningham, "Enhanced fluorescence emission from quantum dots on a photonic crystal surface," Nat. Nanotechnol. **2**(8), 515–520 (2007).
6. F. Tam, G. P. Goodrich, B. R. Johnson, and N. J. Halas, "Plasmonic enhancement of molecular fluorescence," Nano Lett. **7**(2), 496–501 (2007).
7. D. Gérard, J. Wenger, A. Devilez, D. Gachet, B. Stout, N. Bonod, E. Popov, and H. Rigneault, "Strong electromagnetic confinement near dielectric microspheres to enhance single-molecule fluorescence," Opt. Express **16**(19), 15297–15303 (2008).
8. L. C. Estrada, O. E. Martinez, M. Brunstein, S. Bouchoule, L. Le-Gratiet, A. Talneau, I. Sagnes, P. Monnier, J. A. Levenson, and A. M. Yacomotti, "Small volume excitation and enhancement of dye fluorescence on a 2D photonic crystal surface," Opt. Express **18**(4), 3693–3699 (2010).
9. E. Usukura, S. Shinohara, K. Okamoto, J. Lim, K. Char, and K. Tamada, "Highly confined, enhanced surface fluorescence imaging with two-dimensional silver nanoparticle sheets," Appl. Phys. Lett. **104**(12), 121906 (2014).

#247952 Received 21 Aug 2015; revised 22 Oct 2015; accepted 22 Oct 2015; published 5 Nov 2015

10. G. Soavi, G. Della Valle, P. Biagioni, A. Cattoni, G. Cerullo, and D. Brida, "Ultrafast non-thermal response of Plasmonic resonance in Gold Nanoantennas," in *CLEO: 2014*, OSA Technical Digest (online) (OSA, 2014), paper FTh4C.7.
11. J. P. Hugonin and P. Lalanne, "Reticolo software for grating analysis," Institut d'Optique, Palaiseau, France (2005).
12. M. G. Moharam, E. B. Grann, D. A. Pommet, and T. K. Gaylord, "Formulation for stable and efficient implementation of the rigorous coupled-wave analysis of binary gratings," J. Opt. Soc. Am. A **12**(5), 1068–1076 (1995).
13. M. G. Moharam, D. A. Pommet, E. B. Grann, and T. K. Gaylord, "Stable implementation of the rigorous coupled-wave analysis for surface-relief gratings: enhanced transmittance matrix approach," J. Opt. Soc. Am. A **12**(5), 1077–1086 (1995).
14. P. Lalanne and G. M. Morris, "Highly improved convergence of the coupled-wave method for TM polarization," J. Opt. Soc. Am. A **13**(4), 779–784 (1996).
15. C. R. Doerr and H. Kogelnik, "Dielectric waveguide theory," J. Lightwave Technol. **26**(9), 1176–1187 (2008).
16. X. S. A. Maier, *Plasmonics: Fundamentals and Aplications* (Springer, 2007), Ch. 5.
17. J. Plain and J. Martin, "Fabrication of aluminium nanostructures for plasmonics," J. Phys. D Appl. Phys. **48**(18), 184002 (2014).
18. C. F. R. Mateus, M. C. Y. Huang, Y. Deng, A. R. Neureuther, and C. J. Chang-Hasnain, "Ultra-broadband mirror using low index cladded subwavelength grating," IEEE Photonics Technol. Lett. **16**(2), 518–520 (2004).
19. H. Hattori, X. Letartre, C. Seassal, P. Rojo-Romeo, J. Leclercq, and P. Viktorovitch, "Analysis of hybrid photonic crystal vertical cavity surface emitting lasers," Opt. Express **11**(15), 1799–1808 (2003).
20. G. W. Bryant, F. J. García de Abajo, and J. Aizpurua, "Mapping the plasmon resonances of metallic nanoantennas," Nano Lett. **8**(2), 631–636 (2008).
21. K. Aydin, V. E. Ferry, R. M. Briggs, and H. A. Atwater, "Broadband polarization-independent resonant light absorption using ultrathin plasmonic super absorbers," Nat. Commun. **2**, 517 (2011).
22. A. Cattoni, M. Faustini, A. Yacomotti, D. Decanini, D. Grosso, and A. M. Maghiri-Gosnet, "Degassing-assisted patterning of Sol-gel derived films: a pressureless technique for low-cost and large-scale replication of nanostructures at the 15 nm scale," in preparation.

1. Introduction

Confinement of fluorescence excitation in small volumes near surfaces is crucial in biology for the study of membrane dynamics and organization in cells. One of the most used techniques to achieve this confinement is Total Internal Reflection Fluorescence Microscopy (TIRFM). This technique is based on the evanescent field (~200 nm penetration depth at $1/e^2$) generated in the upper medium when a beam is totally reflected. To achieve the total internal reflection, the incident beam angle must be higher than the critical angle ($\theta_c \approx 61°$ in the glass/water interface). In common TIRFMs these high angles of incidence are achieved with high numerical aperture objectives or with prisms. These techniques are either expensive or hard to align. In this paper we study different structures that allow axial confinement with normal incidence; therefore they can be used as substrates in any inverted or upright microscope.

Optical resonances in wavelength scale periodic dielectric or metallic structures have been widely applied for: label-free sensing [1–4], fluorescent enhancement [5,6] and excitation volume reduction [7–9], among others. These structures can show high contrasted/large optical resonances and high field enhancement [10]. However, strongly resonant structures, such as the photonic crystals used in [8], need a fine tuning of the excitation laser, which is difficult to achieve due to fabrication tolerance and/or the lack of low-cost, narrow line tunable laser sources at the visible range. Hence, a good candidate able to provide a strong axial confinement with a large bandwidth needs to be found. Ideally, such structures require strong field enhancement near the surface, low resonant transmission, and compatibility with large-scale and low-cost fabrication techniques.

In this paper we have designed, fabricated and characterized TiO_2-based nanoimprinted substrates for axial optical confinement. Their ability to increase image contrast is put into evidence trough a microscopy experiment. We compare their capability to increase the axial resolution to different metallo-dielectric structures via simulations of the electric field distribution. All the structures parameters are chosen so they show resonances at 490 nm, which corresponds to the absorption wavelength of one of the most used markers in biology

#247952 Received 21 Aug 2015; revised 22 Oct 2015; accepted 22 Oct 2015; published 5 Nov 2015

(Enhanced Green Fluorescent Protein, EGFP), making these structures compatible with biological imaging.

2. Operation principle

The ability of a resonant structure to increase image contrast is related to the field enhancement of the excitation at the surface in contact with the biological sample, the transmission at resonance and the penetration depth of the optical field into the sample, Fig. 1(a). The confined fluorescence coming from the resonant confined region needs to be larger compared to the background fluorescence coming from the detection volume. The strength of the background fluorescence is related to the amount of light at the excitation wavelength that penetrates beyond the enhancement region and excites fluorophores deeper than the desired optical section. In order to quantify this in a simple way, we will consider a confocal detection scheme as the one used in [8] (this configuration allows to quantify the detection volume in a simple way). Two different volumes can be identified (Fig. 1(b)): the first one is given by the confined excitation $Ve \sim \pi(D/2)^2\delta$, where D is the illumination spot diameter and δ the field penetration depth; a second one is given by the confocal detection $Vd \sim \pi(D/2)^2\delta'$, where $\delta' = \pi^{1/2}\omega_0\kappa$ with ω_0 the $1/e^2$ Gaussian width of the observation volume in the radial direction and κ being the eccentricity of the confocal volume.

The condition to achieve a good fluorescence confinement is that the contribution to fluorescent signal of the confined excitation volume should be much larger than the background detection volume, hence: $T\delta'/2 \ll \eta\delta$, being T the optical transmission and η the enhancement of the confined energy in the near field with respect to free space. Therefore we can define the magnitude R as the ratio between both contributions:

$$R = \frac{\eta\delta}{T\delta'/2}. \tag{1}$$

The higher R the better the structure for optical sectioning, hence R can be regarded as a figure of merit.

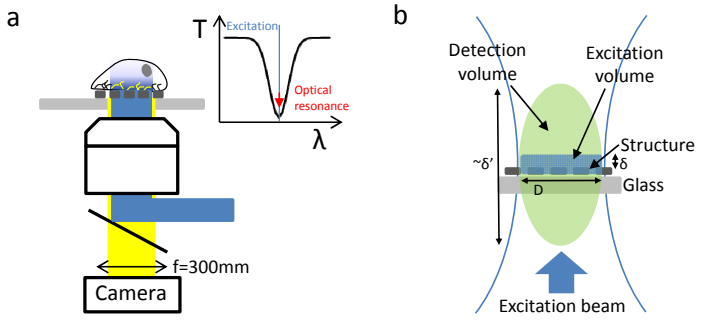

Fig. 1. (a). Sketch of the excitation and detection configuration. Inset: sketch of the resonance spectrum of a structured substrate. (b). Detection and excitation volumes in confocal configuration.

3. Numerical simulations

With the aim of computing R in different resonant photonic systems, we have studied the electric field on the surface of different structures using the software RETICOLO [11]. This free software, written in Matlab 7.0, implements a frequency-domain modal method (known as the Rigorous Coupled Wave Analysis, RCWA) [12–14]. The goal of the simulations was to find the most suitable system for the present application, i.e. to reach a good compromise between strong enhancement on the surface, low incident field transmission and less than 200 nm penetration depth into the upper medium (as in TIRFM).

#247952 Received 21 Aug 2015; revised 22 Oct 2015; accepted 22 Oct 2015; published 5 Nov 2015

Two types of systems were considered, all of them on glass substrates: either dielectric nanostructured planar waveguides or metallic nanostructured layers supporting surface plasmon resonances (SPR). While in dielectric planar waveguides the resonant field enhancement can be explained as a result of multiple constructive interferences [15], in metallic nanostructures, SPRs correspond to coherent oscillations of the surface conduction electrons coupled to the electromagnetic field [16]. The characteristics of the plasmon resonance depend on the nanostructure geometry and the refractive index of the composing materials. Typically the materials used for plasmonics in the IR and near-IR range are gold and silver. In the wavelength of interest for this paper (around 500 nm) these materials are not adequate since gold does not exhibit plasmons resonances in the blue range due to its interband transitions and silver suffers from strong oxidation which degrades its plasmonic properties over time [17]. For this reason we have chosen to use aluminum (Al) due to its compatibility with plasmonics at blue wavelengths [17].

The dielectric structure considered in this work was a 1D grating of TiO_2 stripes (n = 2.35) (Fig. 2). Compared to other geometries such as 2D arrays of air holes, this 1D structure provides large bandwidth resonances [18, 19]. In addition, four metallic (Al) structures were considered: nanorods [20], nanoholes [1], square grating [21], and a sinusoidal grating. All the structures (Fig. 2) lie on glass substrates (n = 1.52) with water on top (n = 1.33). The geometrical parameters are detailed in Table 1. Two polarizations were considered (TE or TM), where TE corresponds to the electric field in Y direction while in TM it is contained in the X-Z plane (Fig. 2(a)); each polarization was chosen in order to obtain the lowest transmission signal at resonance.

Transmitted and reflected signal normalized by the incident intensity are shown in Fig. 2(b). The simulation method computes the transmitted and reflected intensity far away from the surface and it considers material absorption. All the structures show optical resonances at the wavelength of interest (490 nm, black arrow) with different transmission coefficients. It is important to note that depending on the structure, narrow or large resonances are obtained, hence different type of sources can be used for the excitation: e.g. lasers for narrow or large resonances and LEDs for larger resonances. The latter are suitable for the present application since there is a flexible choice of the excitation source and they do not need fine spectral tuning.

The field distribution is shown in Fig. 2(c), where the modulus square of the electric field in the vertical plane (X-Z) at 490 nm is plotted. Hot spots on the surfaces and field decay inside the upper medium can be observed. The details of the field penetration upon the upper medium are depicted in Fig. 2(d) where the intensity profile along the dotted line in Fig. 2(c) is shown. The values shown correspond to the decay at $1/e^2$ of the surface intensity.

Table 1. Parameters values of the simulated structures

Structure	P_x (nm)	P_y (nm)	L_x (nm)	L_y (nm)	h (nm)	h_t (nm)	Polarization
TiO_2	335	-	130	-	180	-	TE
Rods	180	80	105	30	30	-	TM
Holes	355	150	355	150	200	-	TM
Square grating	360	-	180	-	10	100	TM
Sinusoidal grating	360	-	-	-	10	500	TM

Differences in transmission features, field enhancement and penetration depths are due to the fact that dielectric and plasmonic resonances result from different physical mechanisms. In the dielectric structures (TiO_2) the optical resonance results from a coupling of a guided Bloch mode to a radiative mode that propagates perpendicularly to the sample. Here, the enhancement as well as the low transmission are due to optical interference [8,15]. As far as metallic structures are concerned, two different resonances should be distinguished: localized surface plasmons (LSP, rods and holes) and surface plasmon polaritons (SPP, gratings). The attenuated transmission in LSPs is essentially due to extinction (resonant absorption and

#247952 Received 21 Aug 2015; revised 22 Oct 2015; accepted 22 Oct 2015; published 5 Nov 2015

scattering). For SPPs, both the lateral extension and the penetration depth into the dielectric material are typically much larger compared to LSPs (about 270 nm of exponential decay in our case compared to few nm of the LSPs). As the light confinement is much weaker compared to LSPs, the field enhancement is also reduced [16].

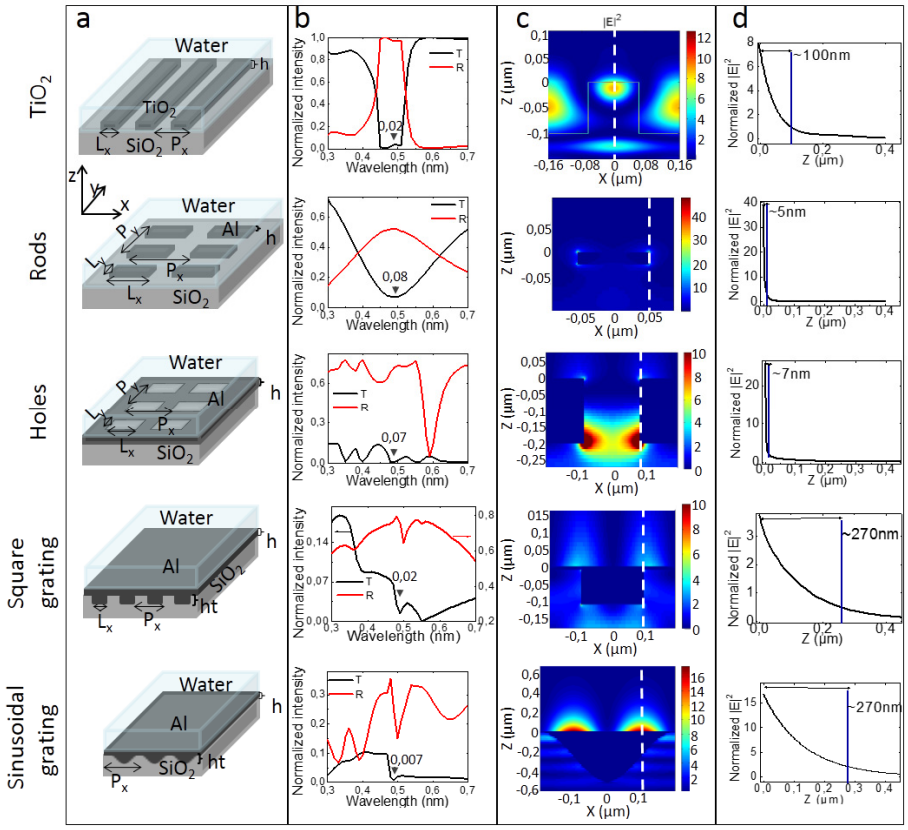

Fig. 2. Sketches of the simulated structures (a). (b). Normalized reflected and transmitted signal. The optical resonances are signed with a black arrow. The numbers correspond to the transmission at resonance. (c). Intensity distribution in the structure. (d). Intensity profiles corresponding to the dotted white lines show in (c). The origin (z = 0) corresponds to the top of the structured substrate.

From Fig. 2(b) we obtain the values of T (transmission at resonance); η is obtained from Fig. 2(d) as the field intensity at the surface (z = 0) and δ [also from Fig. 2(d)] as the penetration depth at $1/e^2$, all these values are shown in Table 2. Both η and δ are computed along a cross-section corresponding to the field maximum (Fig. 2(c), white dashed line). With these values, plotted in Figs. 3(a) and 3(b), and considering δ' = 2µm which corresponds to ω_0~0.2µm (typical value for a confocal microscope), R values for each structure were calculated [Table 2 and Fig. 3(c)].

Table 2. Transmission at resonance (T), field enhancement (η), penetration depth (δ) and calculated R.

Structure	T	η	δ (nm)	R
TiO_2	0.02	7	100	35
Rods	0.08	39	5	2.4
Holes	0.07	26	7	2.6
Square grating	0.02	4	270	54
Sinusoidal grating	0.007	17	270	655

#247952 Received 21 Aug 2015; revised 22 Oct 2015; accepted 22 Oct 2015; published 5 Nov 2015

According to Fig. 3(c), metallic nanorods and nanoholes show decay distances too short for cell imaging applications, and also low R values. Therefore they are not suitable for optical sectioning. The best compromise between field enhancement and low transmission (so better optical confinement) are given by the sinusoidal and square grating structures. However they show penetration depths larger than TIRFM, so they are useful if high confinement is not necessary. Moreover, according to Fig. 2(b), they exhibit low transmission in a wide spectral range, which is inconvenient for transmission imaging. On the contrary, the TiO_2 structure exhibits quite large average transmission in the visible range while preserving large R and higher axial confinement than in TIRFM (still compatible with biological imaging).

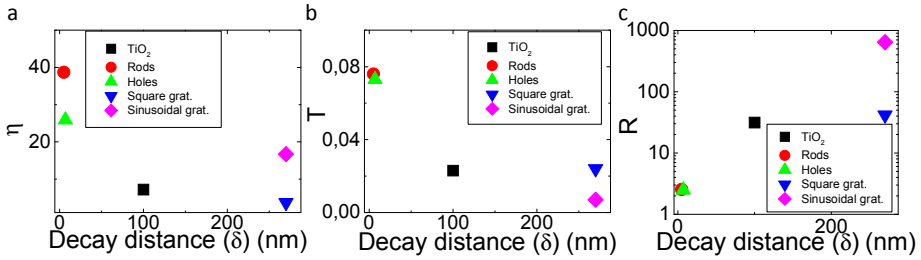

Fig. 3. (a) and (b). Field enhancement (η) and signal transmission (T) at resonance (λ = 490nm) as a function of the decay distance (δ). (c). Values of R (magnitude relating η, T and δ, R = ηδ/(Tδ'/2)) as a function of the decay distance.

4. Experimental results

We fabricated gratings of TiO_2 on a glass substrate by direct embossing of TiO_2 sol-gel derived film using a hard-PDMS/PDMS stamp [22]. A great advantage of using TiO_2 structures is given by the fact that the substrates can be easily cleaned by exploiting the photocatalytic properties of TiO_2. Structures with different line widths (L_x) and grating periods (P_x) but constant thickness (h = 180 nm) were fabricated, Fig. 4(a). Their resonances were optically measured by illuminating the structure normally to the surface with polarized (TE) white light and analyzing its transmission with a spectrometer. Transmission spectrum for different values of P_x, normalized by the transmission through the unpatterned substrate, are shown in Fig. 4(B). Slight differences in resonance features were found as L_X was varied. On the contrary, the resonance shifts to higher wavelengths and its contrast increases as long as P_x was increased. The maximum contrast was found to be 20%. This value differs from the one found in section 3. We attribute this difference to fabrication imperfections, such as the rounded edges of the lines and a thin residual layer of TiO_2 of about 15 nm among the lines. Also, the transmission may be increased due to the depolarization of the incident beam before impinging the sample.

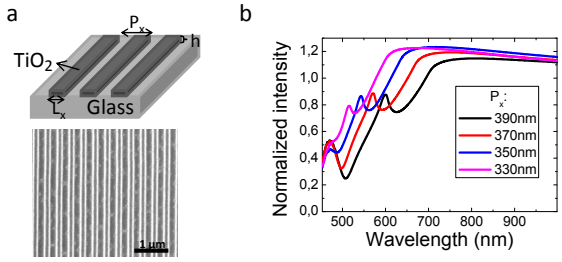

Fig. 4. (a) Top: Sketch of the fabricated TiO_2 nanostructure on glass. Lx: line width, Px: grating period, h: line thickness. Bottom: SEM image of one of the structures. (b) Transmission spectrums of TiO_2 structure for different Px values (Lx = 130nm). Transmitted intensities higher than 1 are due to transmission variation depending on the position on the sample.

#247952 Received 21 Aug 2015; revised 22 Oct 2015; accepted 22 Oct 2015; published 5 Nov 2015

In order to investigate the axial optical sectioning capabilities of the structure, we studied the signal contrast of fluorescent beads (FluoSpheres® Invitrogen, 100 nm diameter, 505/515 nm) deposited on the structure surface and covered with a drop of fluorescein in water (5 µM, 500/515 nm). Images were taken with a blue laser (TE polarization, 470 nm), a 63X objective (1.46 NA Oil, Plan-Apochromat, Zeiss) and a CMOS camera (Zyla, Andor, integration time 100 ms), as schematically shown in Fig. 5(a). From the images, the Weber contrast defined as $C_W = (I_{max}-I_b)/I_{max}$ (I_{max} = peak intensity, I_b = background) was calculated for beads inside and outside the structure, as shown in Fig. 5(b). The contrast varies from 13% (± 5%) outside to 28% (± 9%) inside the patterned region (averaged over 10 measurements) showing that the structure does confine the excitation, being able to increase the image contrast of fluorophores placed at the surface. For comparison, we took images in TIRF condition and a contrast of 48% (± 13%) was found. Therefore, even though the contrast is not as high as in TIRF, within the structure the contrast is higher than double than in an epifluorescence microscope.

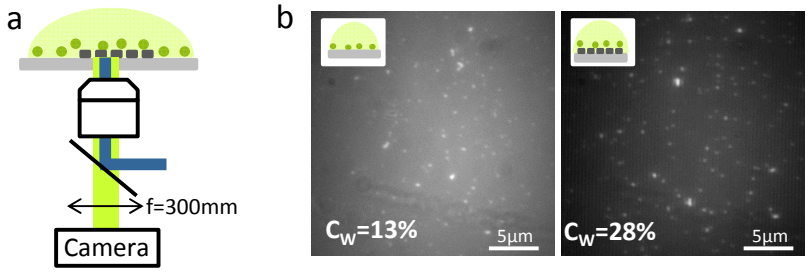

Fig. 5. (a) Experimental set up for image contrast test. (b) Fluorescent beads covered with fluorescein in solution outside (left) and inside (right) the structure (Px = 350nm). The contrast increases more than double within the structure. Note: No degradation of lateral spatial resolution was noticed inside the structure.

5. Conclusions

Field enhancement and confinement in metallic and dielectric structures were numerically simulated with the goal of finding the most suitable structure for optical axial sectioning. By setting a relationship between the field enhancement, transmission at resonance and the decay distance the different structures have been compared. We concluded that two choices are possible depending on the confinement sought; for less than TIRFM axial confinement, the best compromise is given by the sinusoidal metallic grating structure. For higher axial confinement (but still compatible with biological imaging) the best choice is the TiO_2 grating. We fabricated such TiO_2 based structure by direct embossing of a TiO_2 sol-gel derived film on glass using a hard-PDMS/PDMS stamp. Images of fluorescent beads in a fluorescent medium show a twofold signal contrast increase. This contrast could be further improved by optimizing the fabrication process and the illumination conditions. Thus, nanopatterned TiO_2 substrates are promosing structures for optical sectioning without the use of TIRFM.

Acknowledgments

We thank J.P. Hugonin for his help with the numerical simulations, J.-J. Greffet for helpful discussions and Marco Faustini for providing the TiO_2 sol-gel solutions. We acknowledge support and funding from Labex “Ganex” (ANR-11-LBX-0014) and ECOS A13E03.

#247952 Received 21 Aug 2015; revised 22 Oct 2015; accepted 22 Oct 2015; published 5 Nov 2015